Heat Mass Transfer (2016) 52:2813–2821
DOI 10.1007/s00231-016-1784-7

ORIGINAL

Study on effective thermal conductivity of silicone/phosphor composite and its size effect by Lattice Boltzmann method

Lan Li[1] · Huai Zheng[1] · Chao Yuan[1] · Run Hu[1] · Xiaobing Luo[1]

Received: 19 May 2015 / Accepted: 18 February 2016 / Published online: 27 February 2016

Abstract The silicone/phosphor composite is widely used in light emitting diode (LED) packaging. The composite thermal properties, especially the effective thermal conductivity, strongly influence the LED performance. In this paper, a lattice Boltzmann model was presented to predict the silicone/phosphor composite effective thermal conductivity. Based on the present lattice Boltzmann model, a random generation method was established to describe the phosphor particle distribution in composite. Benchmarks were conducted by comparing the simulation results with theoretical solutions for simple cases. Then the model was applied to analyze the effective thermal conductivity of the silicone/phosphor composite and its size effect. The deviations between simulation and experimental results are <7 %, when the phosphor volume fraction varies from 0.038 to 0.45. The simulation results also indicate that effective thermal conductivity of the composite with larger particles is higher than that with small particles at the same volume fraction. While mixing these two sizes of phosphor particles provides an extra enhancement for the effective thermal conductivity.

✉ Xiaobing Luo
luoxb@hust.edu.cn

Lan Li
lilan321@hust.edu.cn

Huai Zheng
zhenghuai8817@sina.com

Chao Yuan
yuanchao@hust.edu.cn

Run Hu
hurun@hust.edu.cn

[1] State Key Laboratory of Coal Combustion, School of Energy and Power Engineering, Huazhong University of Science and Technology, Wuhan 430074, China

Keywords Lattice Boltzmann method · Silicone/phosphor composite · Effective thermal conductivity · Size effect

List of symbols

s	Material symbol
$\mathbf{r}$	Position vector (m)
$\mathbf{e_a}$	Discrete velocity (m s^{-1})
g_a	Distribution function
g_a^{eq}	Equilibrium distribution function
c_p	Specific heat capacity (J kg^{-1} K^{-1})
t	Time (s)
c	Lattice sound speed (m s^{-1})
T	Temperature (K)
q	Heat flux (W m^{-2})
ΔT	Temperature difference (K)
L	Composite thickness (m)
k	Thermal conductivity (W m^{-1} K^{-1})
k_{eff}	Effective thermal conductivity (W m^{-1} K^{-1})
R_b	Interface thermal resistance (m^2 KW^{-1})
d	Particle diameter (m)

Greek symbols

ρ	Density (kg m^{-3})
τ	Dimensionless relaxation time
δ_x	Grain size (m)
δ_t	Time step (s)
ϕ	Volume fraction
α	Dimensionless parameter

Subscripts

n	nth Phase
i	Phase i
j	Phase j
int	Interface

a, b Velocity direction number
p Phosphor particle
s Silicone matrix

1 Introduction

High power light emitting diode (LED) has been considered as a promising light source with the extraordinary characteristics of high luminous efficiency, low power consumption, long lifetime and environment protection [1–3]. Currently, LEDs have been widely applied in daily life, especially in the general lighting market.

The common LED chip can only emit blue light. To realize white light, it's usual to coat the composite of silicone matrix and phosphor powders around blue LED chips in packaging [4]. When the blue light emitted from the LED chip passes through the phosphor composite layer, a part of blue light is absorbed by phosphors, in which the yellow light is emitted. Due to the Stokes loss, the silicone/phosphor composites generate a considerable amount of heat. Owing to the low thermal conductivity of the composite and encapsulant layer, it is difficult to dissipate such a part of heat outside. Thus, there is probably a high local temperature in the phosphor composite layer, which usually causes many problems such as emitting peak shift, color shift, low efficiency and short lifetime [5, 6]. Thus the thermal management in silicone/phosphor composite attracts more and more attention recently. To analyze and solve the heat transfer problem in phosphor composite layer, it is necessary to accurately predict the effective thermal conductivity of the silicone/phosphor composite.

However, few research works were dedicated to the effective thermal conductivity of the silicone/phosphor composite. In the limited literatures, Zhang et al. [7] constructed a finite element model of silicone/phosphor composites by the Monte Carlo method and investigated the influence of the phosphor concentration on the effective thermal conductivity of the phosphor gel layer. In their study, the phosphor volume fraction is only limited within 0.3. Yuan, and Luo [8] built a unit cell model (UCM) to predict the thermal conductivity of the silicone/phosphor composites with considering the interface resistance between the silicone matrix and the phosphor particles. However, this approach leads to a large error at a high volume fraction. What's more, both of their researches don't consider the phosphor particle size influence on the effective thermal conductivity. In fact, the particle size in composite has a strong effect on the effective thermal conductivity for other composites, for example, the boron nitride (BN) filled composites [9, 10]. Therefore, the size effect of phosphor particles is a pressing issue in research.

With the advanced computational techniques, lattice Boltzmann method (LBM) is considered especially suitable to deal with the thermal properties of complex microstructures. Qian et al. [11] proposed a D2Q5 lattice Boltzmann method to investigate the effective thermal conductivity of porous media firstly without considering the solid–fluid conjugate heat transfer. However, the solid–fluid conjugate heat transfer is proved to be a critical factor for predicting the effective thermal conductivity of some composites. In order to deal with the conjugate heat transfer, Wang et al. [12] proposed a mesoscopic lattice Boltzmann algorithm and calculated the effective thermal conductivity of microscale random porous media. The algorithm was applied to predict the effective thermal conductivity for some two-phase and three-phase porous media combined with a random structure generation method. The methodology has been approved to be consistent with experimental data. Besides, effective thermal conductivity of unique structural morphology like carbon fiber composites [13] can be calculated as well. In the research field of size effect, Wang et al. [14, 15] studied the size effect on effective thermal conductivity of porous media with and without the thermal contact resistance. They made a point of view that the effective thermal conductivity decreased sharply as the grain size got smaller when thermal contact resistance was considered. However, the phosphor particles are inconsecutive in the silicone matrix, which is different from porous media. The method to study the size effect on this situation was not discussed in their research, while the work provided an inspiration on the study of silicone/phosphor composites.

Herein, a lattice Boltzmann model was applied to predict the effective thermal conductivity of silicone/phosphor composites in this paper. What's more, a new random structure generation method considering size effect was proposed for silicone/phosphor composites. Then the model was validated through the comparison between the experimental and the simulation results. Size effect of the phosphor particle was also analyzed.

2 Numerical methods

2.1 Silicone/phosphor composite model

In order to accurately calculate the effective thermal conductivity of the silicone/phosphor composites, the key is to numerically describe phosphor particle distribution in composites. A random generation model was applied. Figure 1 shows the scanning electron microscopes (SEMs) of phosphor particles (Fig 1a) and 5 vol% silicone/phosphor composites (Fig. 1b). SEM images of the particles and composites are taken by using Quanta 200 at an accelerating voltage of 5 and 20 kV, respectively. The particles were

sputtered with a thin layer of graphite before imaged. And the composites were polished and coated with a thin layer of gold for better imaging. From these figures, it can be seen that the phosphor particles are randomly distributed in the silicone matrix. Thus the silicone/phosphor composite physical model was established as shown in Fig. 2a. To simplify the generation process, each phosphor particle was simulated as spherical particle and the particle diameter in the physical model was defined as the average grain size. The upper and lower boundaries are isothermal at T_1 and T_2, respectively and the left and right boundaries are insulated.

Because of the weak wetting characteristic, separations exist between the silicone and the phosphor particles essentially. Specially, a thin layer of interface was introduced into the physical model to separate the silicone matrix and the phosphor particles [15]. Figure 2b shows the interface layer, it introduces an effective thermal contact resistance layer in order to investigate the size effect of the phosphor particle.

Figure 3 shows the schematic diagram of a phosphor particle in silicone matrix with the interface layer, the direct connected nodes to the phosphor particle nodes are defined as interface layer instead of silicone matrix. Obviously, the thermal contact resistance is affected by the particle surface area sensitively, which can be reflected by the interface layer. Moreover, it is assumed that the interface layer thickness is not influenced by particle size under the same mixing conditions. In this way, the particle size is controlled by changing the number of nodes in the algorithm. Referred to Fig. 3, a "stair-case" approximation is applied to accommodate the phosphor particles, and the random generation process is described as follows: (1) All the grids are marked as $s = 0$ with the symbol s meaning different material in the composite and 0 representing the silicone matrix. (2) Randomly generate a node (x_0, y_0) as the particle center, and the nodes whose distance to the center are less than the given phosphor particle radius r are assigned as $s = 1$. For the nodes that are just outside the outline of the phosphor particle, the symbol s is defined as $s = 2$ which represents the interface layer. (3) Generate a new particle center and examine whether the symbol s of all the particle including nodes equals to 0, if so, repeat the step (2). (4) Generate phosphor particles randomly until the volume fraction reaches the objective value ϕ. Then the silicone/phosphor composite microstructure can be generated in a random generation method.

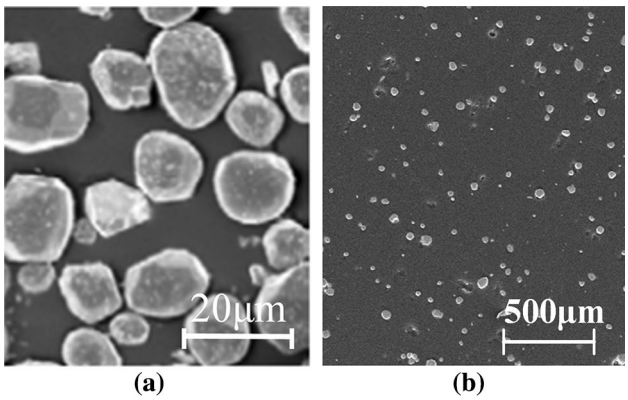

Fig. 1 SEM photographs of phosphor particle (**a**) and silicone/phosphor composite (**b**)

2.2 Lattice Boltzmann algorithm

The energy transport equations for the temperature and heat flux fields should be solved to calculate the effective thermal conductivity of the silicone/phosphor composite. For convenience, the algorithm is introduced in a two-phase situation [16], based on which the silicone matrix and the phosphor particle with the interface layer can be simulated in the same way.

For a steady pure thermal conduction without phase change and convection, the equations for the two-phase structure without heat sources are written as

$$(\rho c_p)_n \left(\frac{\partial T}{\partial t} \right) = k_n \nabla^2 T \tag{1}$$

where the subscript n represents the nth phase, then k_n is the local thermal conductivity of the nth phase, and ρ is

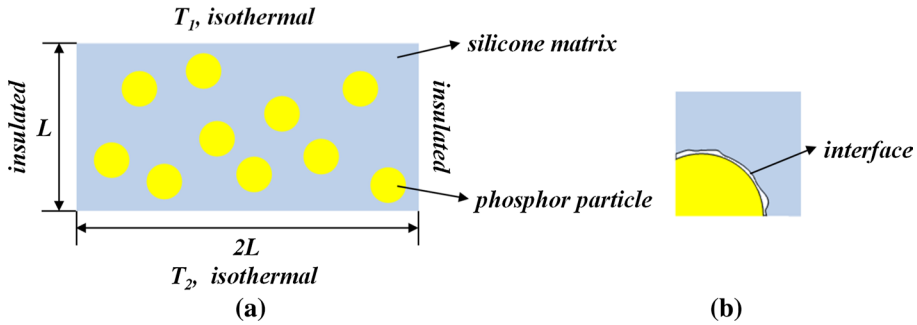

Fig. 2 **a** Schematic diagram of silicone/phosphor composite physical model. **b** The enlarged view of the interface layer

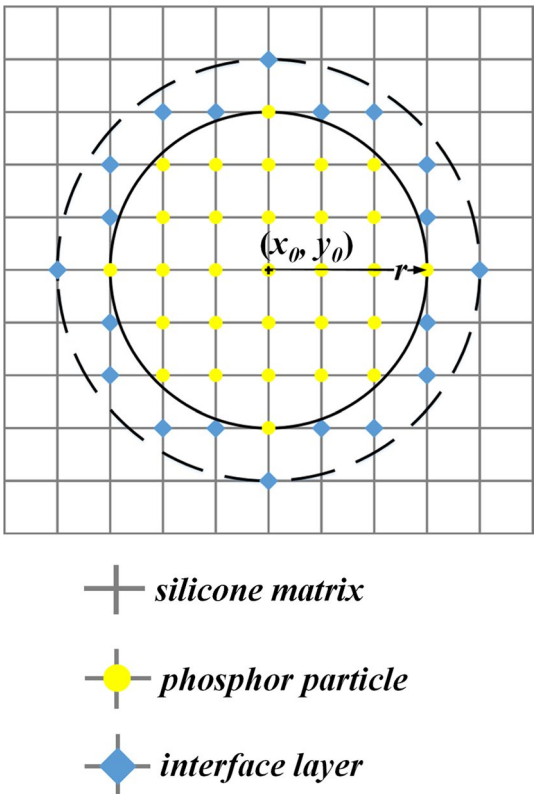

Fig. 3 Schematic diagram of a phosphor particle in silicone matrix with the interface layer

the density, c_p the specific heat capacity, T the temperature, t the time.

The temperature and the heat flux continuities should be satisfied at the inter-phase surfaces between two phases (i and j) are

$$T_{i,\text{int}} = T_{j,\text{int}} \tag{2}$$

$$k_i \left.\frac{\partial T}{\partial \hat{n}}\right|_{i,\text{int}} = k_j \left.\frac{\partial T}{\partial \hat{n}}\right|_{j,\text{int}} \tag{3}$$

where the subscript *int* means the interphases between any two phases i and j.

Based on these equations, the evolution equation can be described as [17, 18]

$$g_a(\mathbf{r} + \mathbf{e_a}\delta_t, t + \delta_t) - g_a(\mathbf{r}, t) = -\frac{1}{\tau_n}[g_a(\mathbf{r}, t) - g_a^{eq}(\mathbf{r}, t)] \tag{4}$$

where g_a is the local distribution in each discrete direction, $\mathbf{r}$ is the position vector, t is the real time, δ_t is the time step, τ_n is the dimensionless relaxation time for local phase, and $\mathbf{e_a}$ is the discrete velocity. For the simulation model, we compared the two dimensional model and three dimensional model and found that both of the modelling results were close to the experimental data. While the 3D simulation takes more than 200 times grids and very long time, and what's more, the calculation is very complex. In the basic level of acceptable deviation limitation, 2D simplification is applied. So the two-dimensional nine-speed (D2Q9) model is chosen to improve the computational efficiency, in which $\mathbf{e_a}$ is

$$\mathbf{e_a} = \begin{cases} (0,0), & a = 0 \\ (\cos\theta_a, \sin\theta_a)c, & \theta_a = (\alpha - 1)\pi/2, \quad a = 1 - 4 \\ \sqrt{2}(\cos\theta_a, \sin\theta_a)c, & \theta_a = (\alpha - 5)\pi/2 + \pi/4, \quad a = 5 - 8 \end{cases} \tag{5}$$

And the corresponding equilibrium distribution function g_a^{eq} is given by

$$g_a^{eq} = \begin{cases} 0, & a = 0 \\ \frac{T}{6}, & a = 1 - 4 \\ \frac{T}{12}, & a = 5 - 8 \end{cases} \tag{6}$$

The dimensionless relaxation time τ_n in Eq. (4) is decided by the thermal conductivity of each material as

$$\tau_n = \frac{3}{2}\frac{k_n}{(\rho c_p)_n c^2 \delta_t} + 0.5 \tag{7}$$

In order to ensure the continuity at the inter-phase surface [19], under the premise of correctness the volume thermal capacities (ρc_p) should be set as

$$(\rho c_p)_i = (\rho c_p)_j \tag{8}$$

And c is the lattice sound speed defined as

$$c = \frac{\delta_x}{\delta_t} \tag{9}$$

with δ_x the grid size.

The value of c can take any positive value to make sure the value of τ_n within (0.5, 2) [20]. Then the macroscopic variables temperature and heat flux can be calculated as [21]

$$T = \sum_a g_a \tag{10}$$

$$q = \left(\sum_a \mathbf{e_a} g_a\right)\frac{\tau_n - 0.5}{\tau_n} \tag{11}$$

Once the temperature and the heat flux are solved, the effective thermal conductivity k_{eff} is determined as

$$k_{eff} = \frac{qL}{\Delta T} \tag{12}$$

where q is the steady heat flux across the composite section between the temperature difference ΔT with the distance L.

2.3 Boundary conditions

There are two kinds of boundaries in this silicone/phosphor composite model in lattice Boltzmann method. To deal with the isothermal boundary, a bounce-back rule of the non-equilibrium distribution proposed by Zou and He [22] is applied. Then the isothermal boundary can be described as

$$g_a - g_a^{eq} = -(g_b - g_b^{eq}) \tag{13}$$

where the subscripts a and b represent the opposite discrete velocity directions and the equilibrium distribution function g^{eq} can be obtained by the Eq. (10) on the boundary.

For the insulated boundary, the Neumann boundary treatment is chosen to ensure that the boundary temperature gradient equals to zero [23]. While this can lead to energy leak along the insulated surfaces, to avoid that a specula reflection treatment is introduced here as

$$g_a = g_b \tag{14}$$

3 Results and discussion

3.1 Benchmarks

The lattice Boltzmann method and the codes were validated according to some simple models which have theoretical solutions. Figure 4 shows the two models. In Fig. 4, the parallel model and the series model are the basic thermodynamic models whose effective thermal conductivities are $(k_1 + k_2)/2$ and $1/(1/2k_1 + 1/2k_2)$ in theory, respectively. k_1 and k_2 are the thermal conductivities for these two components.

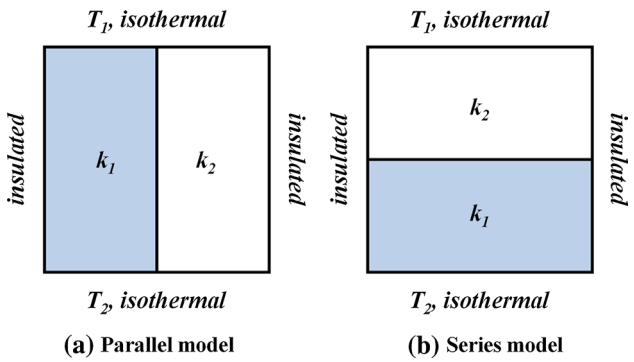

Fig. 4 Two models with theoretical solutions. **a** Parallel model. **b** Series model

Since that the thermal conductivities of the silicone matrix and phosphor particle is 0.16 and 13 W/m K respectively, for the validation if the algorithm could work under such a conductivity contrast, k_1 was kept as 0.16 W/m K with k_2 changing as 0.32, 1.6, 3.2, 16, 32 W/m K respectively. The simulation results compared with the theoretical solutions were listed in Table 1. Table 1 shows that the relative deviations are no larger than 0.251 % which are in the range of permitted errors. The comparison indicates that the lattice Boltzmann method for silicone/phosphor composites is accurate.

3.2 Effective thermal conductivity of the silicone/phosphor composites

In this calculation, the thermal conductivities of the silicone matrix and the phosphor particle are 0.16 and 13 W/m K. And the simulation was performed under the condition that $T_1 = 300$ K, and $T_2 = 290$ K with a 400 μm × 200 μm computational domain. The mean size of the phosphor particle was 13 μm. Changing the volume fraction of phosphor as 0.038, 0.075, 0.158, 0.25, 0.35 and 0.45 respectively, the effective thermal conductivity of the silicone/phosphor composites was simulated. Experiments under the same conditions were also done in our previous work in Ref. [8]. In the experiments, the experimental equipment uncertainty is 3 %, and to increase the experimental accuracy, all the samples were measured for five times under each volume fraction and the mean value of them were calculated.

The grid independence proof was done. Figure 5 presents the effect of grid number on the effective thermal conductivity at the phosphor volume fraction of 0.038, 0.158 and 0.45. The abscissa of Fig. 5 is the grid number in the thickness direction, and the ordinate is the calculated

Table 1 The comparison between the simulation results and the theoretical solution

k_1 (W/m K)	k_2 (W/m K)	Parallel model			Series model		
		Theoretical solution (W/m K)	Simulation result (W/m K)	Relative deviations (%)	Theoretical solution (W/m K)	Simulation result (W/m K)	Relative deviations (%)
0.16	0.32	0.240	0.240	0.000	0.2133	0.2134	0.047
0.16	1.6	0.880	0.880	0.000	0.2909	0.2912	0.103
0.16	3.2	1.680	1.680	0.000	0.3048	0.3053	0.164
0.16	16	8.080	8.079	0.012	0.3168	0.3175	0.221
0.16	32	16.080	16.078	0.012	0.3184	0.3192	0.251

effective thermal conductivity. In Fig. 5, with grid number increasing, the curves are close to horizontal lines, which proves the simulation convergence. A 400 × 200 grid is finally chosen to guarantee the computation accuracy and save the calculation time. Besides, to avoid the random distribution influence on the effective thermal conductivity, the average values of effective thermal conductivity under 200 and 1000 iterations were compared both at the lowest and the highest volume fractions. With only a deviation of 0.28 %, a total of 200 iterations were performed to obtain a representative simulation result.

The comparison between the simulation results and the experimental data at different volume fraction was shown in Fig. 6. The abscissa of Fig. 6 is the volume fraction of the phosphor particles, while the ordinate is the effective thermal conductivity of the silicone/phosphor composites. In Fig. 6, we also compared our results with the effective thermal conductivity prediction models [24, 25].

For the Maxwell–Garnett model,

$$\frac{k_{eff}}{k_s} = \frac{[k_p(1+2\alpha)+2k_s]+2\phi[k_p(1-\alpha)-k_s]}{[k_p(1+2\alpha)+2k_s]-\phi[k_p(1-\alpha)-k_s]} \tag{15}$$

where ϕ is the volume fraction and α is the dimensionless parameter written as

$$\alpha = \frac{2R_b k_s}{d} \tag{16}$$

where R_b is interface thermal resistance between the particles and the matrix and d is the particle diameter.

For the Bruggeman asymmetric model,

$$(1-\phi)^3 = \left(\frac{k_{eff}}{k_s}\right)^{\frac{1+2\alpha}{1-\alpha}} \times \left\{\frac{k_{eff}-k_p(1-\alpha)}{k_s-k_p(1-\alpha)}\right\}^{\frac{3}{1-\alpha}} \tag{17}$$

The Bruggeman asymmetric model is typically used for spherical particles with high volume fraction.

Nonlinear curve fitting by minimizing the deviations between the simulation results and the model predictions is applied to determine the value of α, which represents the particle size and interface effect. Based on the least-square algorithm, α equals to 0.08 when the volume fraction is low, while 0.032 at a high volume fraction. The difference may result from the direct contact between particles.

From Fig. 6, it can be found that the LBM predictions agree with the experimental data well at the volume fraction from 0.038 to 0.45, which is real fraction range in silicone/phosphor composite applications. And the detailed deviation analysis was given in Table 2. Table 2 indicates that the relative deviation is no larger than 6.761 %.

Figure 6 also shows that the effective thermal conductivity is enhanced with the volume fraction increasing. The effective thermal conductivity increases slowly when the volume fraction is lower than 0.2, while it has a sharp

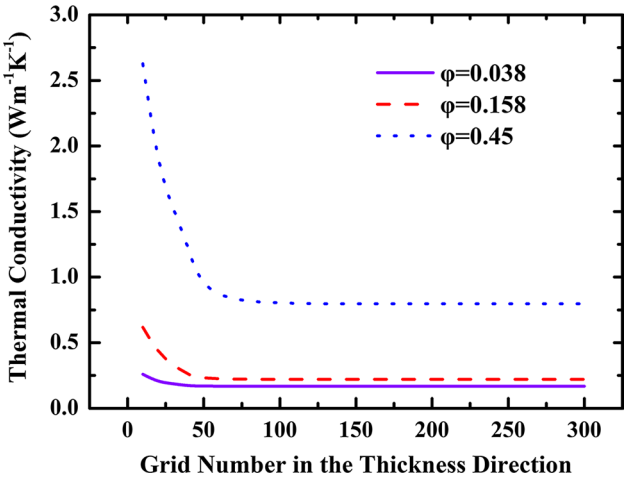

Fig. 5 The effect of grid number in the thickness direction on the effective thermal conductivity

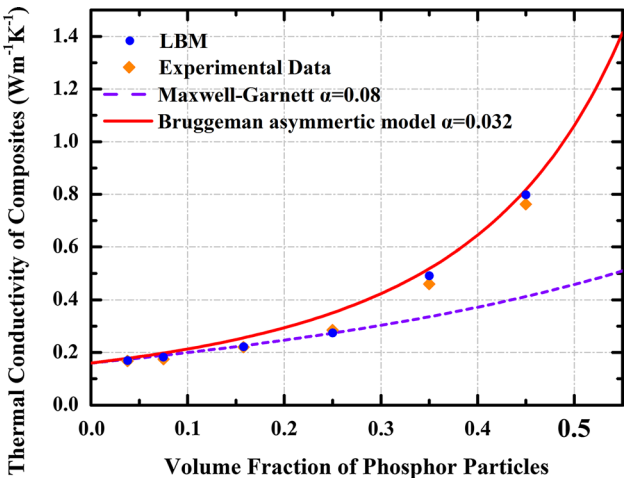

Fig. 6 Comparison between the simulation results and the experimental data

increase after that. Compared with prediction models, we also found that when the volume fraction is low, the LBM results match to the Maxwell–Garnett modeling (dash line) well. It is usually believed that the Maxwell–Garnett model [26] is especially suitable for spherical particles with $\phi < 0.4$ [27]. In Fig. 6, it is also found that when the volume fraction reaches at 0.35, the results match to the Bruggeman asymmetric model (solid line) [28]. This model is typically used for spherical particles with high volume fraction.

3.3 Size effect of the silicone/phosphor composites

To investigate how the phosphor particle size affects the effective thermal conductivity, a thin interface layer is

Table 2 Deviation analysis between the simulation and experimental results

Volume fraction of phosphor	Simulation result (W/m K)	Experimental result (W/m K)	Relative deviations (%)
0.038	0.1689	0.1680	0.536
0.075	0.1820	0.1750	4.000
0.158	0.2215	0.2200	0.682
0.25	0.2737	0.2850	3.965
0.35	0.4911	0.4600	6.761
0.45	0.7975	0.7629	4.535

Table 3 Different cases for investigating size effect

Case	(1)	(2)	(3)	(4)	(5)
d (μm)	4	8	12	16	n_1:n_4 = 2:1

introduced into the model with its thermal conductivity k_{int} as 0.01 W/m K [15]. The simulations were done under different particle sizes as: (1) $d_1 = 4$ μm; (2) $d_2 = 8$ μm; (3) $d_3 = 12$ μm; and (4) $d_4 = 16$ μm. They are cases (1) to (4) respectively. In case (5), the ratio of the 4 μm-diameter particle number to the 16 μm-diameter particle number is 2–1. All the cases are listed in Table 3. In all of these five cases, the volume fraction of the phosphor changed as 0.075, 0.158, 0.25, 0.35 and 0.45.

The simulation comparison under different phosphor particle sizes was illustrated in Fig. 7. The abscissa and the ordinate are the volume fraction of phosphor particles and the effective thermal conductivity as well. And the triangular, square, obtriangular and circular represent four different phosphor particle sizes respectively.

Figure 7 shows that the effective thermal conductivity with the larger phosphor particle size is higher than that of a small particle size under the same volume fraction. The same phenomenon can be found in porous materials [14, 15]. The increase can be explained as follows: The larger the phosphor particle, the lower the specific surface area it is, which leads to less scattering phenomenon in thermal barrier. When the particle size decreases, the particles can't be able to contact well with each other, and the thermal contact resistance dominates the heat transfer process.

To analyze the size effect intensity on the effective thermal conductivity, using 4 μm-diameter particle as base, the thermal conductivity growth were illustrated in Fig. 8. Figure 8 shows that the size effect of the silicone/phosphor composites is more obvious at a higher volume fraction, and this indicates that the phosphor particle size doesn't play an important role for the effective thermal conductivity of silicone/phosphor composites at low volume fraction when there are not enough particles to contact with each other.

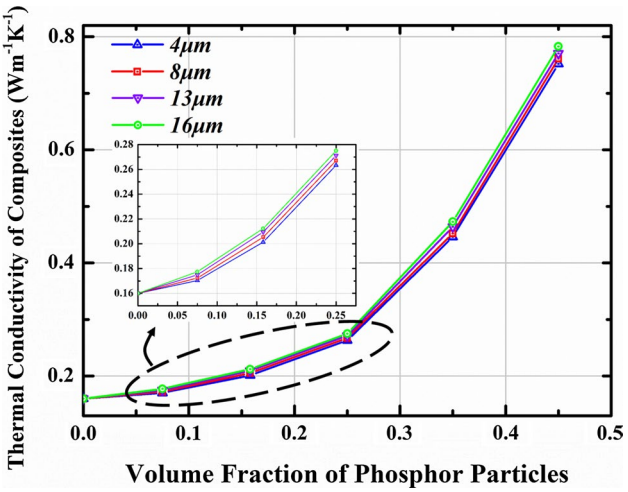

Fig. 7 The simulation result comparison under different phosphor particle sizes

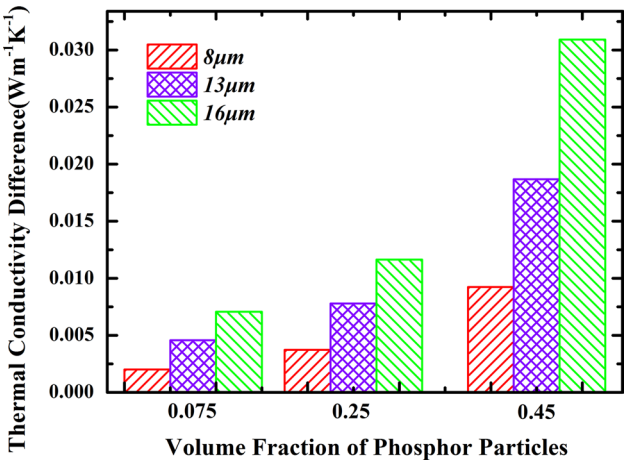

Fig. 8 The comparison of the effective thermal conductivity using 4 μm-diameter particle as base

In addition, the effective thermal conductivity of case (5) was compared with case (1) and (4). The comparison results are listed in Table 4. Here, the increase rate is calculated as

Table 4 Effective thermal conductivity comparison between case (5) and case (1) and (4)

Volume fraction of phosphor	Effective thermal conductivity (W/m K)			Increase rate (%)
	Case (1)	Case (4)	Case (5)	
0.075	0.17035	0.17742	0.17925	3.128
0.158	0.20134	0.21226	0.21463	3.859
0.25	0.26332	0.27497	0.27912	3.755
0.35	0.44617	0.47314	0.48239	5.037
0.45	0.75189	0.78281	0.80903	5.475

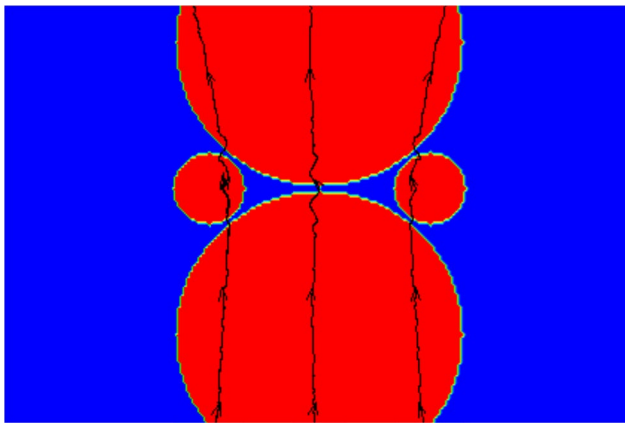

Fig. 9 Heat streaming lines when different particle sizes are mixed

$$Increase\ rate = \frac{1}{2}\left[\left(\frac{k_{eff5} - k_{eff1}}{k_{eff1}}\right) + \left(\frac{k_{eff5} - k_{eff4}}{k_{eff4}}\right)\right] \quad (18)$$

From Table 4, we find that under the condition that the small phosphor particles and the large phosphor particles are mixed, the effective thermal conductivity becomes higher. The reason is that the small phosphor particles can make up the space of the large particles, and this can increase the contact surfaces and escape from the air void. By means of mixing, particles can make alignment and provide more heat pathway across the composites [29]. Figure 9 shows the heat streaming lines and it proves the above conclusion.

4 Conclusions

A lattice Boltzmann model was applied to predict the effective thermal conductivity of silicone/phosphor composites with a random structure generation method. Based on the benchmark validations, the lattice Boltzmann method was applied to predict the effective thermal conductivity of the silicone/phosphor composites. Compared with our published experimental work, the lattice Boltzmann model can provide an accurate prediction at the volume fraction from 0.038 to 0.45. The simulation results also show a better consistency with existing thermal conductivity prediction models. The size effect of the phosphor particle was also analyzed using this method. The simulation results also indicate that effective thermal conductivity of the composite with larger particle is higher than that with small particle at the same volume fraction. While mixing these two sizes of phosphor particles provide an extra enhancement for the effective thermal conductivity.

Acknowledgments The authors would like to acknowledge the financial support partly by National Science Foundation of China (51376070), and partly by 973 Project of The Ministry of Science and Technology of China (2011CB013105).

References

1. Liu S, Luo X (2011) LED packaging for lighting applications: design, manufacturing, and testing. Wiley, New York
2. Zukauskas A, Shur M, Gaska R (2002) Introduction to solid state lighting. Wiley, New York
3. Pimputkar S, Speck JS, DenBaars SP, Nakamura S (2009) Prospects for LED lighting. Nat Photon 3:180–182
4. Hu R, Yu S, Zou Y, Zheng H, Wang F, Liu S, Luo X (2013) Near-/mid-field effect of color mixing for single phosphor-converted light-emitting diode package. IEEE Photon Technol Lett 25:246–249
5. Narendran N, Gu Y, Freyssinier J, Yu H, Deng L (2004) Solid-state lighting: failure analysis of white LEDs. J Cryst Growth 268:449–456
6. Fan B, Wu H, Zhao Y, Xian Y, Wang G (2007) Study of phosphor thermal-isolated packaging technologies for high-power white light-emitting diodes. IEEE Photon Technol Lett 19:1121–1123
7. Zhang Q, Pi Z, Chen M, Luo X, Xu L, Liu S (2011) Effective thermal conductivity of silicone/phosphor composites. J Compos Mater 45(23):2465–2473
8. Yuan C, Luo X (2013) A unit cell approach to compute thermal conductivity of uncured silicone/phosphor composites. Int J Heat Mass Transf 56:206–211
9. Zhou W, Qi S, Li H, Shao S (2007) Study on insulating thermal conductive BN/HDPE composites. Thermochim Acta 452:36–42
10. Zhou WY, Qi SH, Zhao HZ, Liu NL (2007) Thermally conductive silicone rubber reinforced with boron nitride particle. Polym Compos 28:23–28
11. Qian J, Li Q, Yu K, Xuan Y (2004) A novel method to determine effective thermal conductivity of porous materials. Sci China Ser E Technol Sci 47:716–724
12. Wang M, Wang J, Pan N, Chen S (2007) Mesoscopic predictions of the effective thermal conductivity for microscale random porous media. Phys Rev E 75:036702
13. Wang J, Wang M, Li Z (2007) A lattice Boltzmann algorithm for fluid–solid conjugate heat transfer. Int J Therm Sci 46:228–234
14. Wang M, Pan N, Wang J, Chen S (2007) Mesoscopic simulations of phase distribution effects on the effective thermal conductivity of microgranular porous media. J Colloid Interface Sci 311:562–570
15. Wang M, Wang X, Wang J, Pan N (2013) Grain size effects on effective thermal conductivity of porous materials with internal thermal contact resistance. J Porous Media 16(11):1043–1048

16. Wang M, Pan N (2008) Predictions of effective physical properties of complex multiphase materials. Mater Sci Eng R Rep 63:1–30
17. Peng Y, Shu C, Chew Y (2003) Simplified thermal lattice Boltzmann model for incompressible thermal flows. Phys Rev E 68:026701
18. Chen X, Han P (2000) A note on the solution of conjugate heat transfer problems using SIMPLE-like algorithms. Int J Heat Fluid Flow 21:463–467
19. Wang J, Wang M, Li Z (2006) Lattice Poisson–Boltzmann simulations of electro-osmotic flows in microchannels. J Colloid Interface Sci 296:729–736
20. Kang Q, Zhang D, Lichtner PC, Tsimpanogiannis IN (2004) Lattice Boltzmann model for crystal growth from supersaturated solution. Geophys Res Lett 31:L21604
21. D'Orazio A, Succi S (2003) Boundary conditions for thermal lattice Boltzmann simulations. In: Computational Science — ICCS 2003, vol 2657. Springer, Berlin, Heidelberg, pp 977–986
22. Zou Q, He X (1997) On pressure and velocity boundary conditions for the lattice Boltzmann BGK model. Phys Fluids (1994-present) 9:1591–1598
23. D'Orazio A, Corcione M, Celata GP (2004) Application to natural convection enclosed flows of a lattice Boltzmann BGK model coupled with a general purpose thermal boundary condition. Int J Therm Sci 43:575–586
24. Prasher R (2006) Thermal interface materials: historical perspective, status, and future directions. Proc IEEE 94:1571–1586
25. Karayacoubian P, Yovanovich M, Culham J (2006) Thermal resistance-based bounds for the effective conductivity of composite thermal interface materials. In: Semiconductor thermal measurement and management symposium, 2006 IEEE twenty-second annual IEEE, IEEE, pp 28–36
26. Davis L, Artz B (1995) Thermal conductivity of metal-matrix composites. J Appl Phys 77:4954–4960
27. Nan C-W, Birringer R, Clarke DR, Gleiter H (1997) Effective thermal conductivity of particulate composites with interfacial thermal resistance. J Appl Phys 81:6692–6699
28. Every A, Tzou Y, Hasselman D, Raj R (1992) The effect of particle size on the thermal conductivity of ZnS/diamond composites. Acta Metall Mater 40:123–129
29. Liu J, Wang T, Carlberg B, Inoue M (2008) Recent progress of thermal interface materials. In: Electronics system-integration technology conference, 2008. ESTC 2008. 2nd, IEEE, pp 351–358